Interaction of atom with nonparaxial Laguerre-Gaussian beam: Forming superposition of vortex states in Bose-Einstein condensates

Anal Bhowmik,[1] Pradip Kumar Mondal,[2] Sonjoy Majumder,[1,*] and Bimalendu Deb[3]
[1]*Department of Physics, Indian Institute of Technology Kharagpur, Kharagpur-721302, India*
[2]*Department of Applied Science, Haldia Institute of Technology, Haldia-721657, India*
[3]*Department of Materials Science, Indian Association for the Cultivation of Science, Jadavpur, Kolkata 700032, India*
(Received 2 February 2016; published 28 June 2016)

The exchange of orbital angular momentum (OAM) between paraxial optical vortex and a Bose-Einstein condensate (BEC) of atomic gases is well known. In this paper, we develop a theory for the microscopic interaction between matter and an optical vortex beyond paraxial approximation. We show how superposition of vortex states of BEC can be created with a focused optical vortex. Since the polarization or spin angular momentum (SAM) of the optical field is coupled with OAM of the field, in this case, these angular momenta can be transferred to the internal electronic and external center-of-mass motion of atoms provided both the motions are coupled. We propose a scheme for producing the superposition of matter-wave vortices using Gaussian and a focused Laguerre-Gaussian beam. We study how two-photon Rabi frequencies of stimulated Raman transitions vary with focusing angles for different combinations of OAM and SAM of optical states. We demonstrate the formation of vortex-antivortex structure and discuss interference of three vortex states in a BEC.

DOI: 10.1103/PhysRevA.93.063852

I. INTRODUCTION

Recognition of orbital angular momentum (OAM) of light has evoked a lot of activities in different branches of physics over the past two decades. Spin angular momentum (SAM) is carried by the polarization of light, while OAM is by helical phase front. Being an extrinsic property, OAM generally affects the center-of-mass (c.m.) motion of an atom, whereas SAM of field determines the selection rules of electronic transitions. In our recent work [1], we have shown that optical OAM can be transferred to electronic motion via quantized c.m. motion of ultracold atoms within paraxial approximation. For focused optical vortex beam, parxial approximation breaks down and nonparaxial effects [2] become important. A new realm of physics can be explored for atoms or molecules interacting with a nonparaxial (focused) optical vortex where the SAM and the OAM are no longer conserved separately but the total angular momentum (OAM+SAM) is conserved in interaction with an atom or a molecule [3,4]. The interesting feature of focused optical vortex is that the OAM of light can be transferred to the electronic motion or the SAM of light can affect the c.m. motion of an atom even at dipole approximation level unlike that in the case of paraxial approximation. Considering direct coupling of field OAM with the internal motion of atoms, many applications are proposed in literature, such as second-harmonic generation in nonlinear optics [5], new selection rules in photoionization [6–8], strong dichroism effect [9,10], charge-current generation in atomic systems [11], the suppression of parasitic light shifts in the field of quantum information and metrology experiments with single atoms or ions [8], new selection rules in off-axis photoexcitation [12], etc. The nonparaxial vortex beams have applications in different fields of research, such as quantum information processing [13], trapping of atoms [14] or microparticles [15] in optical twizers, cell biology [16], etc.

Here we develop a theory for the interaction of a nonparaxial vortex beam with an atom and apply this to the creation of superposition of matter wave vortices in an atomic Bose Einstein condensate (BEC). We show the possibility to create multiple quantized circulations of BEC using single focused optical vortex pulse, unlike that in earlier works [17–19] where multiple optical vortices were used. To transfer the OAM from the light to the c.m. motion of matter, the wavelength of the matter wave has to be large enough to feel the intensity distribution of the optical vortex beam. So, this theory will be applicable to cold atoms. Since the spread of wave function of a cold single trapped atom is very narrow, a transfer mechanism is appreciable for a large number of cold atoms, like BEC. The main question we address in this paper is about the sharing mechanism of the total angular momentum of a focused optical vortex between the external c.m. and internal electronic motions of an atom. We show that there are three possible ways of distributing the total field angular momentum between c.m. and electronic motions. We call them angular momentum channels (AMC) of interaction. The atoms interact with the LG beam via different AMCs having probabilities that depend on corresponding transition strengths and focusing angles.

The formalism of corresponding interaction is developed in Sec. II. Section III describes numerical calculations of a proposed method of creation of superposition of BEC vortex states using nonparaxial LG beam. Section IV discusses some examples of superposition of BEC vortex states, like the vortex-antivortex pair, which can be created by our proposed method giving simulated interference patterns. Finally, in Sec. V, we make some concluding remarks.

II. THEORY

The focused nonparaxial beam considered here is produced from a circularly polarized paraxial pulse with OAM by passing it through a lens with high numerical aperture (NA). The consequent spin-orbit coupling of light is based on Debye-

*sonjoym@phy.iitkgp.ernet.in

Wolf theory [20,21], where an incident collimated LG beam is decomposed into a superposition of plane waves having an infinite number of spatial harmonics. In a nonparaxial beam, the total angular momentum is a good quantum number. In the rest of the paper, whenever we mention SAM or OAM, it should be understood that we mean the corresponding angular momentum of the paraxial LG beam before passing through the lens. We consider that the focused LG_p^l beam (l is OAM of light beam [2] and p is radial node of Laguerre polynomial) interacts with cold atoms whose de Broglie wavelength is large enough to feel the intensity variation of the focused beam. For nonparaxial circularly polarized LG_0^l beam, the x,y,z-polarized component of the electric field [4,22,23] in the laboratory coordinate system can be expressed as

$$E_x(r',\phi',z') = (-i)^{l+1}E_0\big(e^{il\phi'}I_0^{(l)} + e^{i(l+2\beta)\phi'}I_{2\beta}^{(l)}\big), \quad (2.1)$$

$$E_y(r',\phi',z') = \beta(-i)^l E_0\big(e^{il\phi'}I_0^{(l)} - e^{i(l+2\beta)\phi'}I_{2\beta}^{(l)}\big), \quad (2.2)$$

$$E_z(r',\phi',z') = -2\beta(-i)^l E_0 e^{i(l+\beta)\phi'}I_\beta^{(l)}, \quad (2.3)$$

where β is the polarization of light incident on the lens. Here, we consider only circular polarization with $\beta = \pm 1$. The amplitude of the focused electric field is $E_0 = \frac{\pi f}{\lambda}T_o E_{\rm inc}$, where we have assumed T_o is the objective transmission amplitude, $E_{\rm inc}$ is the amplitude of incident electric field, and f is the focal length related with r' by $r' = f\,\sin\theta$ (Abbe sine condition). The coefficients $I_m^{(l)}$, where m takes the values 0, ± 1, ± 2 in the above expressions depend on focusing angle ($\theta_{\rm max}$) by [4]

$$I_m^{(l)}(r'_\perp,z') = \int_0^{\theta_{\rm max}} d\theta\left(\frac{\sqrt{2}r'_\perp}{w_0\sin\theta}\right)^{|l|}(\sin\theta)^{|l|+1} \times \sqrt{\cos\theta}\,g_{|m|}(\theta)J_{l+m}(kr'_\perp\sin\theta)e^{ikz'\cos\theta}, \quad (2.4)$$

where $r'_\perp$ is the projection of $\mathbf{r}'$ on the xy plane, w_0 is the waist of the paraxial beam, and $J_{l+m}(kr'_\perp\sin\theta)$ is the cylindrical Bessel function. The angular functions are $g_0(\theta) = 1+\cos\theta$, $g_1(\theta) = \sin\theta$, and $g_2(\theta) = 1-\cos\theta$.

We consider the above field interacts with simplest atomic system with a core of total charge $+e$ and mass m_c and a valence electron of charge $-e$ and mass m_e. The c.m. coordinate with respect to laboratory coordinate system is $\mathbf{R} = (m_e\mathbf{r}_e + m_c\mathbf{r}_c)/m_t, m_t = m_e + m_c$ being the total mass and their relative (internal) coordinate is given by $\mathbf{r} = \mathbf{r}_e - \mathbf{r}_c$ [1]. Here $\mathbf{r}_e$ and $\mathbf{r}_c$ are the coordinates of the valence electron and the center of atom, respectively, with respect to laboratory coordinate system.

The atomic system is trapped in a harmonic potential and the atomic state can be written as a product of the c.m. wave function and electronic wave function $\Upsilon(\mathbf{R},\mathbf{r}) = \Psi_R(\mathbf{R})\psi(\mathbf{r})$. The c.m. wave function $\Psi_R(\mathbf{R})$ depends on the external harmonic trapping potential. The internal electronic wave function $\psi(\mathbf{r})$ can be considered as a highly correlated coupled-cluster state [24]. The interaction Hamiltonian $H_{\rm int}$ is derived using the Power-Zienau-Wooley (PZW) scheme [25]. Since $|\mathbf{r}| \ll |\mathbf{R}|$, we can use the Taylor's expansion for the electric field about $\mathbf{R}$. For circularly polarized light, with OAM $= +1$, the electric dipole interaction Hamiltonian becomes [see Appendix, Eq. (A8)]

$$H_{\rm int}^{l=+1,\beta=\pm1} = e\frac{m_c}{m_t}r\sqrt{\frac{8\pi}{3}}\big[-I_0^{(1)}(R_\perp,Z)e^{i\Phi}\epsilon_{\pm1}Y_1^{\pm1}(\hat{\mathbf{r}}) - I_{\pm2}^{(1)}(R_\perp,Z)e^{i(1\pm2)\Phi}\epsilon_{\mp1}Y_1^{\mp1}(\hat{\mathbf{r}}) \pm\sqrt{2}iI_{\pm1}^{(1)}(R_\perp,Z)e^{i(1\pm1)\Phi}\epsilon_{=0}Y_1^0(\hat{\mathbf{r}})\big]. \quad (2.5)$$

Here $H_{\rm int}$ depends mainly on two parameters, i.e., orbital (l) and spin (β) angular momentum of light. The electric dipole transition selection rule is $\Delta l_e = \pm 1$ and $\Delta m_l = 0, \pm 1$. Here l_e and m_l are the electronic orbital angular momentum and its projection along the direction of propagation of the light, i.e., laboratory z axis. In interaction with paraxial beam, any one of the above conditions for Δm_l is satisfied, depending on the polarization of light ($\beta = 0,\pm1$) and we have only one AMC of interaction. But in interaction with nonparaxial light all the possibilities of Δm_l open up for $\beta = 1$ or -1. These generate three possible electronic hyperfine sublevels, as discussed later, in the atoms of BEC as seen from Eq. (2.5). But total angular momentum has to be conserved. Therefore, as seen from the equation, we get three possible orbital angular momentum states of the c.m. of the atoms corresponding to the above electronic states.

Let us now discuss each term of Eq. (2.5) to understand how the SAM and OAM of the incident paraxial beam are shared between the electronic and c.m. motion of the atom. The first term of this equation represents the paraxial term, i.e., the OAM of light interacts with the c.m. motion and the polarization of light interacts with the electronic motion of the atom [5,6,26]. But the second and third terms of this equation imply that the polarization of the light can also affect the external motion of c.m. of the atoms. The three terms sequentially represent three channels referred to as AMC-1, AMC-2, and AMC-3, respectively. With the increase of the focusing, light changes its vector properties and the possibilities of conversion of SAM to OAM increases [3,4]. This implies that AMC-2 and AMC-3 will become more significant with increasing the focusing angle by changing the NA of the lens. One part of the total angular momentum (TAM) goes to the c.m. and creates the vorticity of the matter wave. If any part of TAM goes to the electron, it generates electronic transitions satisfied by the electromagnetic selection rules. Therefore, the dipole transition matrix element between two states ($|\Upsilon_i\rangle$ and $|\Upsilon_f\rangle$) of the system is given by

$$\begin{aligned}M_{i\to f}^d &= \langle\Upsilon_f|H_{\rm int}^{l=+1,\beta=\pm1}|\Upsilon_i\rangle \\ &= e\frac{m_c}{m_t}\sqrt{\frac{8\pi}{3}}\big[-\epsilon_{\pm1}\langle\Psi_{R,f}|I_0^{(1)}(R_\perp,Z)e^{i\Phi}|\Psi_{R,i}\rangle \\ &\quad\times\langle\psi_f|rY_1^{\pm1}(\hat{\mathbf{r}})|\psi_i\rangle - \epsilon_{\mp1}\langle\Psi_{R,f}|I_{\pm2}^{(1)} \\ &\quad\times(R_\perp,Z)e^{i(1\pm2)\Phi}|\Psi_{R,i}\rangle\langle\psi_f|rY_1^{\mp1}(\hat{\mathbf{r}})|\psi_i\rangle \\ &\quad\pm\sqrt{2}i\epsilon_0\langle\Psi_{R,f}|I_{\pm1}^{(1)}(R_\perp,Z)e^{i(1\pm1)\Phi}|\Psi_{R,i}\rangle \\ &\quad\times\langle\psi_f|rY_1^0(\hat{\mathbf{r}})|\psi_i\rangle\big]. \end{aligned} \quad (2.6)$$

The three terms in Eq. (2.6) correspond to vorticities l, $l\pm2$, $l\pm1$, respectively, as seen from the first factors. Second factors correspond to the transition matrix elements for electrons. These factors are numerically evaluated (see Sec. IV) after

estimating the wave functions of c.m. and electronic states of the system. In the next section, we study two-photon stimulated Raman transition using a focused LG beam and predict interesting effects.

III. CREATION OF SUPERPOSITION OF BEC VORTEX STATES

Generation of quantized vortices in a BEC using optical vortex has become important due to the experimental endeavors [27,28] over the past decade. The coherent superpositions of vortices of different circulation quantum numbers, especially vortex-antivortex cases [28,29], yield interesting interference effects with potential applications [30,31], such as manipulating the chirality of twisted metal nanostructures [32]. Creation of matter-wave vortex states from a nonrotating BEC by two-photon Raman transition method under paraxial LG and Gaussian (G) pulse is well discussed in literature [27–30,33–44]. In these studies, matter-wave vortex is shown to acquire vorticity equal to the winding number of the LG beam.

We consider a focused LG beam is interacting with a nonrotating ^{23}Na BEC, prepared in $|\psi_i\rangle = |3S_{\frac{1}{2}}, F = 1, m_f = -1\rangle$ state in a harmonic potential. The LG pulse induces dipole transitions in atoms as given in Eq. (2.6). The final state will have three different hyperfine sublevels shown in Fig. 1. To bring back the matter in the initial state using two-photon stimulated Raman transition, we require three simultaneous copropagating Gaussian pulses with suitable frequencies and polarizations to be shined in the same direction of LG field as shown in Fig. 2. Because of copropagation of the Gaussian pulses with LG field, net transfer of linear momentum to the atoms is zero. Two-photon transitions of matter state through the three hyperfine sublevels of excited state can be defined as three channels discussed below. This procedure yields the possibility of three vorticities in the BEC and creates the superposition of vortices at the initial hyperfine sublevel. Since the interference pattern of the superposition will depend on the populations of the vortex states, the Rabi frequencies

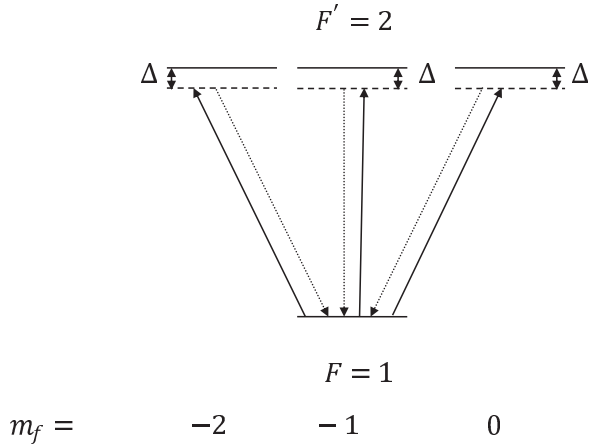

FIG. 1. Energy-level scheme of the two-photon transitions. The atomic states show the ^{23}Na hyperfine states. Atoms are initially in $|3s_{\frac{1}{2}} F = 1, m_f = -1\rangle$. Δ represents two-photon detuning.

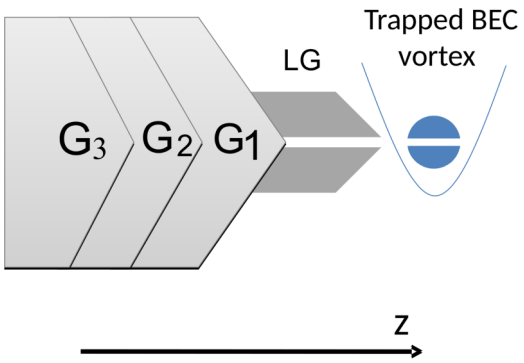

FIG. 2. Single LG and three Gaussian (G_1, G_2, G_3) pulses are applied to BEC.

corresponding to these two-photon transitions are important to quantify.

For axial confinement of the trap, the quantum state of the condensate can be described by a wave function $\Psi(X,Y,t)$ in two dimensions. In the zero-temperature limit, the dynamics of the weakly interacting BEC is described by the Gross-Pitaevskii equation in cylindrical coordinate system. Let us consider a nonparaxial LG beam, produced from a paraxial LG field with OAM $= +1$ and SAM $= +1$, and followed by Gaussian beams incident on BEC. As a result, a superposed vortex state with vorticity $\kappa = 1,2,3$ will be created. In general, the three different macroscopic vortices with vorticities l, $l+\beta$, $l+2\beta$ (originated from OAM $= l$ and SAM $= \beta$) superpose with arbitrary proportion and this superposition can be expressed as [17]

$$\Psi(R,\Phi,t) = f(R)e^{-i\mu t}(\alpha_1 e^{il\Phi} + \alpha_2 e^{i(l+2\beta)\Phi} + \alpha_3 e^{i(l+\beta)\Phi}), \tag{3.1}$$

where $R^2 = (X^2 + Y^2)$ and μ is the chemical potential of the system. α_1, α_2, and α_3 are constants, depended on the strengths of two-photon transitions corresponding to different vortex channels with $|\alpha_1|^2 + |\alpha_2|^2 + |\alpha_3|^2 = 1$. Interestingly, for the combination of (OAM,SAM) $= (1,-1)$ or $(-1,1)$ of incident field, we get superposition of vortex states of BEC in the trap with $\kappa = 0,1,-1$. Therefore, this turns out to be a unique approach to create a superposed state of vortex-antivortex from a single LG beam.

IV. NUMERICAL RESULTS AND INTERPRETATION

We start with single photon scattering by trapped atoms as expressed in Eq. (2.6). For numerical calculations, we choose the characteristics of the experimental trap as given in Ref. [27] with asymmetry parameter $\lambda_{tr} = \omega_Z/\omega_\perp = 2$ and the axial frequency $\omega_Z/2\pi = 40$ Hz. The characteristic length and s-wave scattering length are $a_\perp = 4.673$ μm and $a = 2.75$ nm, respectively. The intensity of the paraxial LG beam, which has been focused, is $I = 10$ mW m^{-2} and its waist $w_0 = 10^{-4}$ m. We now numerically evaluate the Rabi frequencies of dipole transitions considering the Eqs. (2.6) where the c.m. and electronic motions are coupled. Let us consider a left circularly polarized paraxial LG beam (means SAM $= +1$) with OAM $= +1$ that transforms into nonparaxial LG beam and interacts with a nonrotating BEC of 10^5 ^{23}Na atoms in an

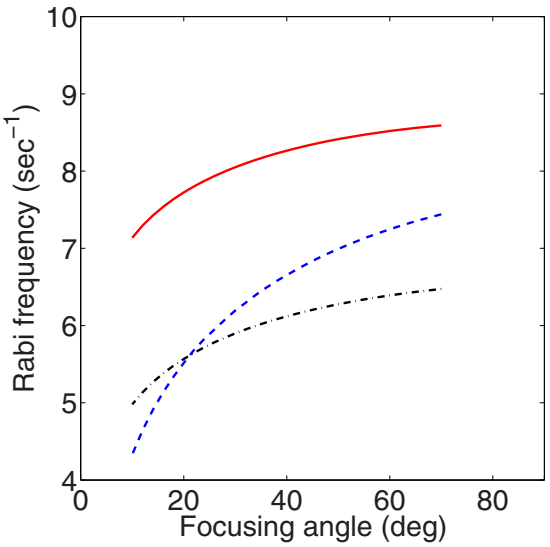

FIG. 3. Variations of dipole Rabi frequency (in sec^{-1}) with focusing angles (in deg) are plotted on a semilog scale. Red solid line refers to electronic transition $|F=1,m_f=-1\rangle$ to $|F'=2,m_f=-2\rangle$, blue dashed line is for $|F=1,m_f=-1\rangle$ to $|F'=2,m_f=0\rangle$, and dotted line represents $|F=1,m_f=-1\rangle$ to $|F'=2,m_f=-1\rangle$.

anisotropic harmonic trap. The axes of the beam and the trap are along the z axis of the laboratory frame.

In Eq. (2.6), $\langle\psi_f|rY_1^{0,\pm1}(\hat{\mathbf{r}})|\psi_i\rangle$ is the electronic portion of the dipole transition due to the interaction with LG beam, but interestingly depends on the vorticity of c.m. motion of BEC. The vorticity of excited state with hyperfine sublevels $m_f=0,-1,-2$ will be l, $l+1$, $l+2$ for SAM $=+1$ of the paraxial field.

Figure 3 shows the Rabi frequencies of different transitions with LG field of OAM $=+1$ and SAM $=-1$. These results show that the values of matrix elements of two-photon transitions increase significantly with focusing angles. Note that $|F=1,m_f=-1\rangle \rightarrow |F=2,m_f=0\rangle$ and $|F=1,m_f=-1\rangle \rightarrow |F=2,m_f=-1\rangle$ transitions are negligible under paraxial approximation. Here, in the nonparaxial case, we notice that these transitions are non-negligible and become significant with high focusing angles. The finiteness of these two transitions at small focusing angle ($\approx10^\circ$) may be due to the inclusion of a diffraction feature during the conversion of paraxial to nonparaxial beam. Interestingly, the relative strength of these two weak transitions changes as we change the focusing angle. The similar features for other combinations of OAM and SAM of light are also observed and will be discussed below.

To calculate the two-photon Rabi frequencies, we consider that copropagating LG and a set of Gaussian (G) beams interact with the trapped BEC as shown in Fig. 2. Let us consider the atoms which will take part in the two-photon transitions will reach final electronic state $|3S_{\frac{1}{2}}F=1,m_f=-1\rangle$. This means the final internal atomic state will be the same as the initial one which is low field seeking. The frequency difference between the two kinds of pulses, $\delta\nu_r$, is the recoil energy. Here G beam is detuned from the D1 line by $\Delta=-1.5$ GHz (≈-150 linewidths, enough to prevent any

TABLE I. Magnitude of Rabi frequencies (in MHz) of two-photon Raman transitions for different focusing angles of incident beam of OAM $=+1$ and SAM $=-1$. κ is the final vorticity of atoms in BEC.

Focusing angle	$\Omega_1(\kappa=1)$	$\Omega_2(\kappa=-1)$	$\Omega_3(\kappa=0)$
70°	456.50	13.17	2.47
60°	386.46	8.46	2.04
50°	303.41	4.69	1.56
40°	215.14	2.15	1.09
30°	131.34	0.75	0.65
20°	61.94	0.16	0.31
10°	15.95	0.01	0.08

significant spontaneous photon scattering). We apply LG/G beams to the trapped atoms and look for the superposition of vortex states. Table I shows the results of two-photon Raman transitions with three channels going through three intermediate states, $\Omega_1=|F'=2,m_f=-2\rangle$, $\Omega_2=|F'=2,m_f=0\rangle$, and $\Omega_3=|F'=2,m_f=-1\rangle$. As expected from the single LG photon absorption, Ω_1 is always greater than Ω_2 and Ω_3. But crossing of amplitudes of Ω_2 and Ω_3 happens at $\approx30^\circ$, unlike single photon transition (which happened at $\approx20^\circ$). The point to be noted here is that Ω_1 and Ω_2 correspond to vorticities 1 and -1, respectively. At high focusing angle, the ratio between the strength of Ω_1 and Ω_2 decreases and an interference pattern will clearly be visible as a superposition of vortex and antivortex, as shown in Fig. 4.

In Table II, the Rabi frequencies are calculated, considering OAM $=+1$ and SAM $=+1$ of paraxial field. Here, the three channels with different intermediate states are $\Omega_4=|F'=2,m_f=0\rangle$, $\Omega_5=|F'=2,m_f=-2\rangle$, and $\Omega_6=|F'=2,m_f=-1\rangle$ with vorticities 1, 3, and 2, respectively. Therefore, a superposition of these three vortex states is possible with comparable combination from each of them. At

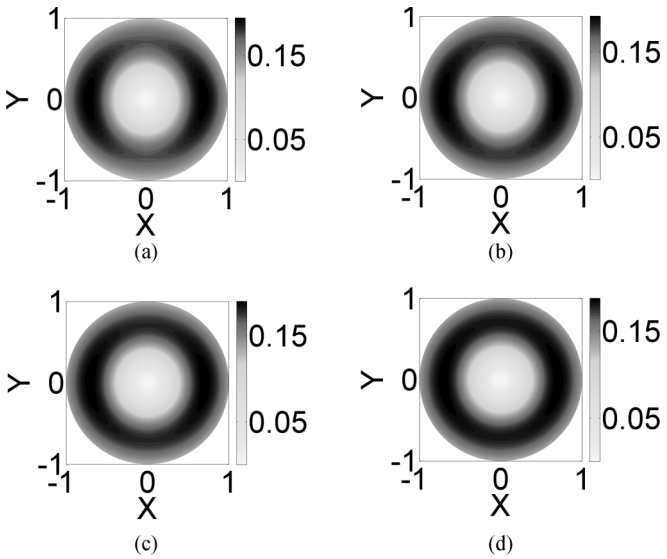

FIG. 4. Plot of the density distribution of vortex antivortex states for focusing angles (a) 70°, (b) 60°, (c) 50°, and (d) 40°. All quantities are in dimensionless units.

TABLE II. Magnitude of Rabi frequencies (in MHz) of two-photon Raman transitions for different focusing angle of incident beam of OAM = +1 and SAM = +1. κ is the final vorticity of atoms in BEC.

Focusing angle	$\Omega_4(\kappa=1)$	$\Omega_5(\kappa=3)$	$\Omega_6(\kappa=2)$
70°	7.61	6003.60	367.31
60°	6.44	3302.00	248.12
50°	5.06	1370.10	144.74
40°	3.59	433.79	69.33
30°	2.19	89.26	24.33
20°	1.03	8.69	5.27
10°	0.27	0.14	0.35

high focusing angle, vortex states corresponding to $\kappa = 2$ and 3 dominate over $\kappa = 1$, which is the only possible vortex state when the LG beam is nonfocused. Also, Table II shows that, at higher focusing angle, the Rabi frequency Ω_5 dominates over the same to Ω_6 and the crossover between the two frequencies takes place at focusing angle $\approx 20^\circ$.

V. CONCLUSION

We have developed the theory of interaction of nonparaxial LG beam with matter. Since OAM and SAM are no longer conserved separately, the interaction can take place through three different orbital angular momentum channels. Therefore, the total angular momentum of optical beam is distributed among the c.m. and electronic motions of atoms in three possible ways. We have prescribed a possible method of creation of superposition of vortex states using single LG pulse and three Gaussian pulses using two-photon stimulated Raman transition. Our numerical calculations estimate the variation of the number of atoms in different vortex states with the focusing angle. At high focusing angle, we see the possibility of an interference pattern created from vortex and antivortex. As we have gone beyond the paraxial limit, many properties of interaction have emerged which can have profound applications in different areas of science and technology in the future.

APPENDIX

The interaction Hamiltonian derived in the (PZW) scheme

$$H_{\rm int} = -\int d\mathbf{r}'\, P(\mathbf{r}') \cdot \mathbf{E}(\mathbf{r}',t) + \text{H.c.}, \tag{A1}$$

where $P(\mathbf{r}')$ is the electric polarization given by

$$P(\mathbf{r}') = -e\frac{m_c}{m_t}\mathbf{r}\int_0^1 d\lambda\, \delta\Big(\mathbf{r}' - \mathbf{R} - \lambda\frac{m_c}{m_t}\mathbf{r}\Big). \tag{A2}$$

We use Taylor's expansion for the electric field about $\mathbf{R}$,

$$E_i\Big(\mathbf{R} + \lambda\frac{m_c}{m_t}\mathbf{r}\Big) = E_i(\mathbf{R}) + \lambda\frac{m_c}{m_t}[\vec{r}\cdot\vec{\nabla}E_i(\mathbf{r})]_{\mathbf{R}} + \cdots. \tag{A3}$$

Here i refers to the x, y, and z component of the electric field. We will use the first part of Taylor's expansion to determine the electric dipole transition. The second part shows the effect of the electric field gradient which finally estimates the electric quadrupole transition. Using Eqs. (A1)–(A3), the interaction Hamiltonian can be written as

$$H_{\rm int} = e\frac{m_c}{m_t}\mathbf{r}\cdot\mathbf{E}\Big(\mathbf{R} + \lambda\frac{m_c}{m_t}\mathbf{r}\Big). \tag{A4}$$

If we are focusing only on the electric dipole transition,

$$\begin{aligned} H_{\rm int} = e\frac{m_c}{m_t}E_0\mathbf{r}\cdot\big[&(-i)^{l+1}I_0^{(l)}(R_\perp,Z)e^{il\Phi}\hat{\mathbf{x}} + (-i)^{l+1}I_{2\beta}^{(l)} \\ &\times(R_\perp,Z)e^{i(l+2\beta)\Phi}\hat{\mathbf{x}} + \beta(-i)^l I_0^{(l)}(R_\perp,Z)e^{il\Phi}\hat{\mathbf{y}} \\ &-\beta(-i)^l I_{2\beta}^{(l)}(R_\perp,Z)e^{i(l+2\beta)\Phi}\hat{\mathbf{y}} \\ &-(2\beta)(-i)^l I_\beta^{(l)}(R_\perp,Z)e^{i(l+\beta)\Phi}\hat{\mathbf{z}}\big]. \end{aligned} \tag{A5}$$

Here, we used the expression of electric-field components from Eqs. (2.1)–(2.3) to determine Eq. (A5). After rearranging this equation,

$$\begin{aligned} H_{\rm int} = e\frac{m_c}{m_t}E_0\mathbf{r}\cdot\big[&I_0^{(l)}(R_\perp,Z)e^{il\Phi}\{\hat{\mathbf{x}}(-i)^{l+1} + \hat{\mathbf{y}}\beta(-i)^l\} \\ &+ I_{2\beta}^{(l)}(R_\perp,Z)e^{i(l+2\beta)\Phi}\{\hat{\mathbf{x}}(-i)^{l+1} - \hat{\mathbf{y}}\beta(-i)^l\} \\ &-(2\beta)(-i)^l I_\beta^{(l)}(R_\perp,Z)e^{i(l+\beta)\Phi}\hat{\mathbf{z}}\big]. \end{aligned} \tag{A6}$$

Now for $l = +1$ and $\beta = \pm 1$, the Hamiltonian has the form

$$\begin{aligned} H_{\rm int}^{l=+1,\beta=\pm1} = e\frac{m_c}{m_t}E_0\mathbf{r}\cdot\big[&-I_0^{(1)}(R_\perp,Z)e^{i\Phi}\{\hat{\mathbf{x}} \pm i\hat{\mathbf{y}}\} \\ &- I_{\pm2}^{(1)}(R_\perp,Z)e^{i(1\pm2)\Phi}\{\hat{\mathbf{x}} \mp i\hat{\mathbf{y}}\} \\ &\pm\sqrt{2}i\,I_{\pm1}^{(1)}(R_\perp,Z)e^{i(1\pm1)\Phi}\hat{\mathbf{z}}\big]. \end{aligned} \tag{A7}$$

Using the condition $\mathbf{r}\cdot\mathbf{E}_0 = r\sqrt{\frac{4\pi}{3}}\sum_{\delta=0,\pm1}\epsilon_\delta Y_1^\delta(\hat{\mathbf{r}})$, with $\epsilon_{\pm1} = (E_x \pm iE_y)/\sqrt{2}$ and $\epsilon_0 = E_z$, we get

$$\begin{aligned} H_{\rm int}^{l=+1,\beta=\pm1} = e\frac{m_c}{m_t}r\sqrt{\frac{8\pi}{3}}\big[&-I_0^{(1)}(R_\perp,Z)e^{i\Phi}\epsilon_{\pm1}Y_1^{\pm1}(\hat{\mathbf{r}}) \\ &- I_{\pm2}^{(1)}(R_\perp,Z)e^{i(1\pm2)\Phi}\epsilon_{\mp1}Y_1^{\mp1}(\hat{\mathbf{r}}) \\ &\pm\sqrt{2}i\,I_{\pm1}^{(1)}(R_\perp,Z)e^{i(1\pm1)\Phi}\epsilon_{=0}Y_1^0(\hat{\mathbf{r}})\big]. \end{aligned} \tag{A8}$$

[1] P. K. Mondal, B. Deb, and S. Majumder, Phys. Rev. A **89**, 063418 (2014).

[2] L. Allen, M. W. Beijersbergen, R. J. C. Spreeuw, and J. P. Woerdman, Phys. Rev. A **45**, 8185 (1992).

[3] L. Marrucci, C. Manzo, and D. Paparo, Phys. Rev. Lett. **96**, 163905 (2006).

[4] Y. Zhao, J. S. Edgar, G. D. M. Jeffries, D. McGloin, and D. T. Chiu, Phys. Rev. Lett. **99**, 073901 (2007).

[5] L. C. Dávila Romero, D. L. Andrews, and M. Babiker, J. Opt. B **4**, S66 (2002).
[6] A. Picón, J. Mompart, J. R. Vázquez de Aldana, L. Plaja, G. F. Calvo, and L. Roso, Opt. Express **18**, 3660 (2010).
[7] A. Picón, A. Benseny, J. Mompart, J. R. Vázquez de Aldana, L. Plaja, G. F. Calvo, and L. Roso, New J. Phys. **12**, 083053 (2010).
[8] C. T. Schmiegelow and F. Schmidt-Kaler, Eur. Phys. J. D **66**, 157 (2012).
[9] M. van Veenendaal and I. McNulty, Phys. Rev. Lett. **98**, 157401 (2007).
[10] P. K. Mondal, B. Deb, and S. Majumder, Phys. Rev. A **92**, 043603 (2015).
[11] K. Köksal and J. Berakdar, Phys. Rev. A **86**, 063812 (2012).
[12] A. Afanasev, C. E. Carlson, and A. Mukherjee, Phys. Rev. A **88**, 033841 (2013).
[13] J. Beugnon *et al.*, Nat. Phys. **3**, 696 (2007).
[14] S. Chu, J. E. Bjorkholm, A. Ashkin, and A. Cable, Phys. Rev. Lett. **57**, 314 (1986).
[15] A. Ashkin, J. M. Dziedzic, J. E. Bjorkholm, and S. Chu, Opt. Lett. **11**, 288 (1986).
[16] A. D. Mehta, M. Rief, J. A. Spudich, D. A. Smith, and R. M. Simmons, Science **283**, 1689 (1999).
[17] M. Liu, L. H. Wen, H. W. Xiong, and M. S. Zhan, Phys. Rev. A **73**, 063620 (2006).
[18] L. H. Wen, J.-S. Wang, J. Feng, and H.-Q. Hu, J. Phys. B: At. Mol. Opt. Phys. **41**, 135301 (2008).
[19] L. Wen, Y. Qiao, Y. Xu, and L. Mao, Phys. Rev. A **87**, 033604 (2013).
[20] B. Richards and E. Wolf, Proc. R. Soc. London, Ser. A **253**, 358 (1959).
[21] A. Boivin and E. Wolf, Phys. Rev. **138**, B1561 (1965).
[22] P. B. Monterio, Paulo A. Maia Neto, and H. M. Nussenzveig, Phys. Rev. A **79**, 033830 (2009).
[23] Y. Iketaki, T. Watanabe, N. Bokor, and M. Fujii, Opt. Lett. **32**, 2357 (2007).
[24] P. K. Mondal, N. N. Dutta, G. Dixit, and S. Majumder, Phys. Rev. A **87**, 062502 (2013).
[25] M. Babiker, C. R. Bennett, D. L. Andrews, and L. C. D. Romero, Phys. Rev. Lett. **89**, 143601 (2002).
[26] R. Jáuregui, Phys. Rev. A **70**, 033415 (2004).
[27] M. F. Andersen, C. Ryu, P. Cladé, V. Natarajan, A. Vaziri, K. Helmerson, and W. D. Phillips, Phys. Rev. Lett. **97**, 170406 (2006).
[28] K. C. Wright, L. S. Leslie, and N. P. Bigelow, Phys. Rev. A **77**, 041601(R) (2008).
[29] K. C. Wright, L. S. Leslie, A. Hansen, and N. P. Bigelow, Phys. Rev. Lett. **102**, 030405 (2009).
[30] J. F. S. Brachmann, W. S. Bakr, J. Gillen, A. Peng, and M. Greiner, Opt. Express **19**, 12984 (2011).
[31] G. F. Quinteiro and T. Kuhn, Phys. Rev. B **90**, 115401 (2014).
[32] K. Toyoda, K. Miyamoto, N. Aoki, R. Morita, and T. Omatsu, Nano Lett. **12**, 3645 (2012).
[33] G. Nandi, R. Walser, and W. P. Schleich, Phys. Rev. A **69**, 063606 (2004).
[34] T. P. Simula, N. Nygaard, S. X. Hu, L. A. Collins, B. I. Schneider, and K. Mølmer, Phys. Rev. A **77**, 015401 (2008).
[35] J.-J. Song and B. A. Foreman, Phys. Rev. A **80**, 033602 (2009).
[36] A. Jaouadi, N. Gaaloul, B. Viaris de Lesegno, M. Telmini, L. Pruvost, and E. Charron, Phys. Rev. A **82**, 023613 (2010).
[37] N. Lo Gullo, S. McEndoo, T. Busch, and M. Paternostro, Phys. Rev. A **81**, 053625 (2010).
[38] M. E. Taşgin, Ö. E. Müstecaplioğlu, and L. You, Phys. Rev. A **84**, 063628 (2011), and references therein.
[39] V. E. Lembessis, D. Ellinas, and M. Babiker, Phys. Rev. A **84**, 043422 (2011), and references therein.
[40] R. Kanamoto and E. M. Wright, J. Opt. **13**, 064011 (2011).
[41] A. Ramanathan, K. C. Wright, S. R. Muniz, M. Zelan, W. T. Hill, C. J. Lobb, K. Helmerson, W. D. Phillips, and G. K. Campbell, Phys. Rev. Lett. **106**, 130401 (2011).
[42] G. R. M. Robb, Phys. Rev. A **85**, 023426 (2012).
[43] A. Yu. Okulov, Phys. Lett. A **376**, 650 (2012).
[44] S. Beattie, S. Moulder, R. J. Fletcher, and Z. Hadzibabic, Phys. Rev. Lett. **110**, 025301 (2013), and references therein.